

SINGULARITY-CONSISTENT TELEOPERATION TECHNIQUES FOR REDUNDANT FREE-FLYING ROBOTS

Dragomir N. Nenchev*

Hirosaki University, 3 Bunkyou-cho, Hirosaki, 036-8561 JAPAN

Kazuya Yoshida†

Tohoku University, Aoba-yama 01, Sendai, 980-8579 JAPAN

ABSTRACT

We analyze the performance of a kinematically redundant, 7 DOF free-flying robot under Cartesian velocity telecontrol. It is shown that the system can be easily destabilized when conventional pseudoinverse redundancy resolution is used, which is due to the presence of algorithmic singularities. A singularity-consistent (SC) solution to the problem is proposed that guarantees stability throughout the feasible motion range. Two SC redundancy resolution techniques are compared: one based on the pseudoinverse of the generalized Jacobian, and another one, based on null space minimization of base attitude disturbance. It is shown that although null space minimization outperforms the pseudoinverse approach in terms of disturbance minimization, this is done at the expense of spurious arm motions. And the gain from the minimization is not sufficient to diminish the disadvantage. Thus, it is concluded that SC pseudoinverse control is a very reliable way of redundancy resolution for a teleoperated arm in space.

projects underway, notably the Ranger project in USA¹ and the ETS VII project in Japan². The ETS VII system was successfully launched in November 1997 and a number of breakthrough experiments have been already conducted on orbit.

Special path planning and control techniques have been developed over the years to account for the free-floating satellite base. The lack of a fixed base means that the reaction force induced by the robot arm appears as disturbance from the standpoint of the satellite attitude control system (ACS). The current approach used with the ETS VII system is based on evaluation of the accumulative momentum along the arm trajectory *before* motion execution. When this momentum exceeds the capacity of the ACS actuators (reaction wheels), trajectory re-planning is invoked, resulting usually in slower motion along the same path². It should be emphasized that this technique is based on the momentum conservation principle, and thus, the path planning and control problems can be solved in terms of velocities, without the need to resolve the complete, second-order system dynamics.

INTRODUCTION

Free-flying space robots are expected to play an important role in future space missions, such as maintenance and repair of existing space structures or satellite systems. There have been several

The above approach is tractable and, therefore, consistent with the current technological level, including available on-board computational power. On the other hand, other manipulator path planning and control techniques have been developed which eventually may avoid the trajectory re-planning problem. These techniques are based on disturbance or reaction minimization. It has been pointed out in literature that a possible way to achieve such minimization is to employ kinematic redundancy³.

Kinematic redundancy resolution techniques are usually based on local minimization methods. There are two main groups of algorithms: the extended

*Professor, Department of Intelligent Machines and System Engineering

†Associate Professor, Department of Aeronautics and Space Engineering

Copyright ©1999 by the American Institute of Aeronautics and Astronautics, Inc. All rights reserved.

task-space approach and the null-space approach⁴. In both approaches, the main constraint (the desirable end-effector motion constraint) is augmented with an additional constraint, a so-called “additional task,” to resolve the redundancy. Note that additional constraints are usually nonlinear. In the case of a free-flying robot, for example, the additional task is derived from the momentum conservation equation³, which is a partially nonholonomic motion constraint. Thus, the superposition of the two constraints leads to a highly nonlinear system. As a result, the set of singularities composed of kinematic singularities (inherent to the main motion constraint), additional task singularities (inherent to the additional motion constraint) and singularities due to the interference of the two constraints, increases significantly. This is quite undesirable because local control methods tend to destabilize the system in the neighborhood of a singular point⁴. We note, therefore, that a credible (local) redundancy resolution technique should always address the singularity problem.

The aim of this paper is to examine the performance of a base-attitude-disturbance minimization algorithm in the presence of singularities. The algorithm combines a null space minimization approach (the so-called “reaction null space approach”⁵) with a technique which we developed recently to deal with kinematic singularities. The latter technique, referred to as the “singularity-consistent (SC)” approach⁶, will be applied here for the first time to treat also algorithmic singularities which are due to the additional task, besides the usual kinematic singularities. It should be pointed out that our approach to singularity treatment has some advantages, mainly in terms of stability and parameter tuning, as compared to the well-known “Damped Least-Squares (DLS)” method^{7, 8}. For a detailed comparison, the interested reader is referred to⁹.

BACKGROUND

The free-flying robot model consists of the satellite base and a seven-link serial manipulator arm attached to it. More specifically, in the simulations we will use a model with the kinematic structure of the Robotics Research Corp. 7 DOF arm¹⁰. It is assumed that the momenta of the robot are conserved (there are no external forces). Denote by \mathbf{P} the linear momentum and by \mathbf{L}_g the angular momentum

with respect to the robot centroid. Then we have:

$$\begin{bmatrix} \mathbf{P} \\ \mathbf{L}_g \end{bmatrix} = \mathbf{H}_b \boldsymbol{\Omega} + \mathbf{H}_{b\phi} \dot{\boldsymbol{\phi}} + \begin{bmatrix} \mathbf{0} \\ \mathbf{r}_{gb} \times \mathbf{P} \end{bmatrix} = \text{const} \quad (1)$$

where $\boldsymbol{\phi} \in \mathbb{R}^7$ denotes arm joint coordinates, $\boldsymbol{\Omega} = [\mathbf{v}^T \boldsymbol{\omega}^T]^T$ stands for the spatial velocity of the base, and \mathbf{r}_{gb} is the base centroid position with respect to the system centroid. Matrix

$$\mathbf{H}_b = \begin{bmatrix} \mathbf{H}_v & \mathbf{H}_{v\omega} \\ \mathbf{H}_{v\omega}^T & \mathbf{H}_\omega \end{bmatrix} \in \mathbb{R}^{6 \times 6}$$

is the base inertia matrix, and

$$\mathbf{H}_{b\phi} = \begin{bmatrix} \mathbf{H}_{v\phi}^T & \mathbf{H}_{\omega\phi}^T \end{bmatrix}^T \in \mathbb{R}^{6 \times 7}$$

is a submatrix of the system inertia matrix, which will be referred to as the *inertia coupling matrix*.

The initial state is assumed zero and hence, the constant in the above equation becomes also zero. Below we focus on the angular part of the momentum equation (1). The reason is that the angular component may lead to attitude destabilization. Since the angular momentum, \mathbf{L}_g , is expressed with reference to the system centroid, the linear momentum \mathbf{P} and the base velocity \mathbf{v} can be canceled out:

$$\mathbf{0} = \tilde{\mathbf{H}}_\omega \boldsymbol{\omega} + \tilde{\mathbf{H}}_{\omega\phi} \dot{\boldsymbol{\phi}}, \quad (2)$$

where $\tilde{\mathbf{H}}_\omega = \mathbf{H}_\omega + wS^2(\mathbf{r}_{gb})$ and $\tilde{\mathbf{H}}_{\omega\phi} = \mathbf{H}_{\omega\phi} + wS(\mathbf{r}_{gb})(\partial \mathbf{r}_{gb} / \partial \boldsymbol{\phi})$, w standing for the total mass and $S(\circ)$ denoting an operator transforming a 3 dimensional vector into a 3×3 skew-symmetric matrix.

Each of the two components on the right-hand-side of Equation (2) defines a *partial angular momentum* of the space robot. $\tilde{\mathbf{H}}_\omega \boldsymbol{\omega}$ will be called the *angular momentum of the base*. The other partial momentum, $\tilde{\mathbf{H}}_{\omega\phi} \dot{\boldsymbol{\phi}}$, is related to manipulator motion, and will be referred to as the *coupling angular momentum*, or shortly, the *coupling momentum*.

It is our objective in this work to minimize base angular disturbance. This is the same as requiring $\boldsymbol{\omega}(t) \rightarrow \mathbf{0}$ throughout the arm motion. Thus, two velocity constraint equations can be written as:

$$\mathbf{0} = \tilde{\mathbf{H}}_{\omega\phi}(\boldsymbol{\phi}(t)) \dot{\boldsymbol{\phi}}(t) \quad (3)$$

and

$$\dot{\mathbf{x}}(t) = \mathbf{J}_{GJ}(\boldsymbol{\phi}(t)) \dot{\boldsymbol{\phi}}(t), \quad (4)$$

where $\dot{\mathbf{x}} \in \mathbb{R}^6$ denotes end-effector spatial velocity and $\mathbf{J}_{GJ}(\boldsymbol{\phi}) \in \mathbb{R}^{6 \times 7}$ stands for the *generalized manipulator Jacobian matrix*¹¹.

Note that the above system of two equations is overdetermined, and hence, no exact solution exists. Thus, one has to look for an approximate solution. When speaking of approximation, we have in mind a local method, such as least-squares. The goal can be formulated as minimization of the objective function

$$\|\tilde{H}_{\omega\phi}(\phi(t))\dot{\phi}(t)\|_{W_1} + \|\dot{\mathbf{x}}(t) - \mathbf{J}(\phi(t))\dot{\phi}(t)\|_{W_2} \quad (5)$$

where $\|\circ\|_{W_i}$ denotes weighted Euclidean norm. Note, care must be taken here since the end-effector task space is not a meterizable space in general, unless one imposes certain constraints. The solution to this minimization problem leads to a technique called "improved configuration control"¹².

In this work, we will employ a different type of redundancy resolution. Note that the two velocity equations above are underdetermined, if taken separately. Hence, each of them admits a set of joint velocity vectors $\dot{\phi}$ as a solution. Once these sets are determined, the other equation can be used to derive the unique solution. Thus, one obtains two unique solutions, which are exact solutions to either Equation (3) or Equation (4). This is nothing else than the well-known "task-of-priority" approach¹³.

SINGULARITY-CONSISTENT CARTESIAN VELOCITY CONTROL

In practice, it is important to ensure exact end-effector task performance. In other words, we have to assign higher priority to the end-effector task, and lower priority to the attitude disturbance minimization task. Thus, we derive the set of exact solutions to the end-effector velocity constraint Equation (4), and obtain an unique solution from this set by restricting it via the angular momentum Equation (3). From Equation (4) we have:

$$\dot{\phi}(t) = \mathbf{J}_{GJ}^+(\phi(t))\dot{\mathbf{x}}(t) + \mathbf{n}(\phi(t))\gamma(t), \quad (6)$$

where $(\circ)^+$ denotes the pseudoinverse, $\mathbf{n} \in \mathbb{R}^7$ stands for the null space vector (recall that the degree of redundancy is one, and hence, there is only one nonzero vector in the null space, unless the generalized Jacobian becomes rank-deficient). γ is a scalar variable which is determined as follows. First, substitute the above result into Equation (3) to obtain:

$$\tilde{H}_{\omega\phi}\mathbf{J}_{GJ}^+\dot{\mathbf{x}} + \tilde{H}_{\omega\phi}\mathbf{n}\gamma = 0 \quad (7)$$

and then solve for γ :

$$\gamma = -\mathbf{c}^+ \tilde{H}_{\omega\phi}\mathbf{J}_{GJ}^+\dot{\mathbf{x}}, \quad (8)$$

where the vector $\mathbf{c} \equiv \tilde{H}_{\omega\phi}\mathbf{n}$. The variable γ is substituted back into Equation (6) to obtain the final solution as:

$$\dot{\phi} = \left(\mathbf{I} - \mathbf{n}\mathbf{c}^+ \tilde{H}_{\omega\phi}\right) \mathbf{J}_{GJ}^+ \dot{\mathbf{x}}. \quad (9)$$

The form of this solution is typical for null-space based redundancy resolution.

It is known that the (pseudo)inverse is discontinuous at singular points. One can then expect stability problems to arise due to the two pseudoinverses in the last equation. Care must be taken by operators of space-based robot arms to avoid singular points. While this can be relatively easily done for nonredundant arms, in case of a redundant arm it is more difficult for the operator to comprehend the set of arm singularities. The introduction of algorithmic singularities, which are different from kinematic ones (in our case, algorithmic singularities are introduced via the \mathbf{c}^+ term), further complicates the situation. The operator would be hardly able to comprehend and to avoid all types of singularities. Even computer-supported visualization would be of not much help. Therefore, we give up such type of analysis and prefer to modify the last solution so that discontinuities disappear. Fortunately, this can be done in a straightforward manner.

We will employ the singularity-consistent (SC) approach developed earlier and tested experimentally with a teleoperation system with a nonredundant slave arm^{6, 14}. Note that the two pseudoinverses appearing in Equation (8), are:

$$\mathbf{J}_{GJ}^+ = \mathbf{J}_{GJ}^T (\mathbf{J}_{GJ}^T \mathbf{J}_{GJ}^T)^{-1} \quad (10)$$

and

$$\mathbf{c}^+ = (\mathbf{c}^T \mathbf{c})^{-1} \mathbf{c}^T. \quad (11)$$

Discontinuities are due to the inverse $(\circ)^{-1}$ in each of the above expressions. The inverse can be represented as

$$(\circ)^{-1} = \sigma \text{adj}(\circ), \quad (12)$$

where $\text{adj}(\circ)$ denotes the adjoint, and $\sigma = \frac{1}{\det(\circ)}$. Obviously, in the neighborhood of a singular point, σ tends to infinity and the system can be easily destabilized.

Looking at Equation (9), it becomes apparent that the two pseudoinverses influence the solution in different ways. Consider first \mathbf{J}_{GJ}^+ . In this case, we can simply ignore $\sigma_{GJ} = 1/\det(\mathbf{J}_{GJ}^T \mathbf{J}_{GJ})$ because it is easy to compensate for it via the magnitude of the velocity command vector $\dot{\mathbf{x}}$. Such modification introduces an error along the direction of motion. But

the important point is that there will be no deviation of the end-effector from the spatial path obtained via the original solution (9). Next, consider the \mathbf{c}^+ pseudoinverse. Since this is the pseudoinverse of a vector, we have $\det(\mathbf{c}^T \mathbf{c}) = \mathbf{c}^T \mathbf{c}$ and $\text{adj}(\mathbf{c}^T \mathbf{c}) = 1$. The term $\sigma_c = 1/(\mathbf{c}^T \mathbf{c})$ cannot be simply ignored, as it was the case with σ_{GJ} . What we can do is to restrict it when it reaches a certain small value ϵ .

Equation (9) is rewritten as

$$\dot{\phi} = l \left(\mathbf{I} - \bar{\sigma}_c \mathbf{n} \mathbf{c}^T \tilde{\mathbf{H}}_{\omega\phi} \right) \mathbf{J}_{GJ}^T \text{adj}(\mathbf{J}_{GJ}^{\#} \mathbf{J}_{GJ}^T) \mathbf{S}. \quad (13)$$

where $\bar{\sigma}_c = \sigma_c$ if $\sigma_c > \epsilon$, and $\bar{\sigma}_c = \epsilon$, otherwise. In the above equation, we have decomposed the input command vector $\dot{\mathbf{x}}$ into direction and magnitude. These are expressed respectively via \mathbf{S} – the unit instantaneous screw of the end-effector, and l , such that $\dot{\mathbf{x}} = l\mathbf{S}$. Note, the elements of \mathbf{S} have the same units as those of $\dot{\mathbf{x}}$, while l is dimensionless.

Equation (13) can be analyzed as an autonomous dynamical system, parameterized via the screw \mathbf{S} . It is known that equilibrium points are the critical points of such systems. Fortunately, at a critical point the system will not destabilize since the adjoint vanishes, and motion tends to zero. The solution has an inherent damping property. This is a major advantage of the SC approach, as compared to pseudoinverse techniques, the DLS method inclusively. Such an advantage is especially useful in space, where safety is of major concern.

SIMULATION STUDY

The simulation software used is a MATLAB based free software package for multibody system modeling, SpaceDyn, developed at Tohoku University¹⁵. The free-flying robot model consists of a base-satellite body (body 0) and a 7 DOF manipulator arm attached to it. As already mentioned, we use the kinematic model of the Robotics Research Corp. 7 DOF arm. Kinematic parameters of the arm can be found in¹⁰. Dynamic parameters, including positions of link centroids, link masses and inertias, are presented in the appendix, using the notation of the SpaceDyn package.

In the simulations, a constant input command in terms of both direction \mathbf{S} and magnitude l is applied. The values assigned to the commanded end-effector direction are shown in the following table:

S(1)	S(2)	S(3)	S(4)	S(5)	S(6)
$-1/\sqrt{2}$	0	$-1/\sqrt{2}$	0	0	0
m/s	m/s	m/s	rad/s	rad/s	rad/s

Thus, the end-effector will move along a straight-line path in the $x - z$ plane, with constant orientation. Note also that a constant l ($l = 3$ throughout the simulations) yields a nonzero initial velocity. But it would be easy to obtain zero initial (and final) velocity, if necessary, since the velocity is *scalable* via l .

In the first simulation the initial configuration is arbitrarily chosen as:

$$\phi = [0 \quad -\pi/2 \quad 0 \quad \pi/2 \quad 0 \quad \pi/2 \quad 0]^T [\text{rad}].$$

To illustrate the additional-task singularity problem due to rank deficiency of the generalized Jacobian, we set $\gamma = 0$ in Equation (6), which yields the “conventional” pseudoinverse based solution. Figure 1 displays the joint velocities and the end-effector path in the $x - z$ plane. At the end of the motion instabilities are clearly observed. It is easily verified that this is indeed due to rank deficiency of the generalized Jacobian. For comparison, we repeat the same motion, i.e. with $\gamma = 0$, but using the following SC version of the pseudoinverse based solution:

$$\dot{\phi} = l \mathbf{J}_{GJ}^T \text{adj}(\mathbf{J}_{GJ}^{\#} \mathbf{J}_{GJ}^T) \mathbf{S}. \quad (14)$$

The result is shown in Figure 2. This time, no instabilities are observed. Of course, the singularity still exists, but the behavior is quite different from the previous case: motion tends to zero, which is due to the critical point of the autonomous system. This behavior means that, when approaching the singularity, the operator will find it more and more difficult to drive the end-effector forward, if l is kept constant.

In the next simulation we employ the base attitude disturbance minimization technique, according to Equation (9). We set the threshold $\epsilon = 0.01$. The initial configuration is the same as above. Note, however, that this is not an optimal configuration since it was arbitrarily chosen. Thus, we can expect fast initial motion, which is needed to bring the arm configuration in accord with the minimization criterion. The result is shown in Figure 3. Indeed, there is a very fast arm reconfiguration at the beginning. But the large velocity can be easily scaled down, as already explained. At the end of the motion, the velocity increases again. Analysis shows that this

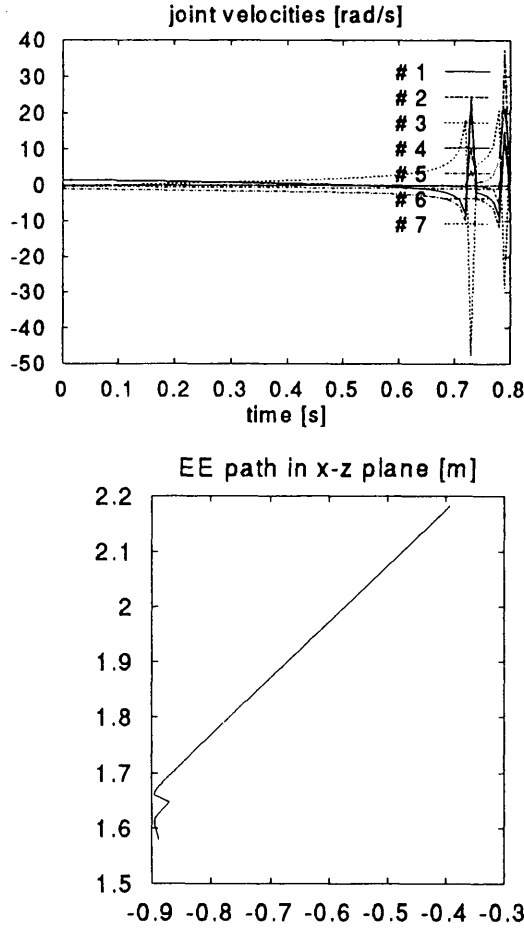


Fig.1: Motion under conventional pseudoinverse control.

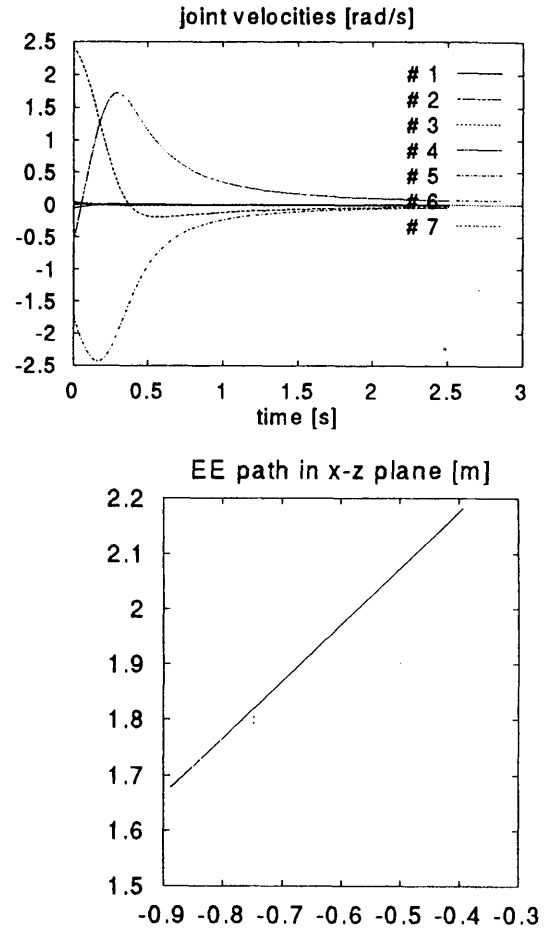


Fig.2: Motion under SC pseudoinverse control.

is due to the vanishing vector \mathbf{c} . This deteriorates the end-effector path as well. In addition, the end-effector cannot travel as far as under SC pseudoinverse control. We performed once again the simulation, but with an initial configuration, close to the optimal one. The data for the new initial configuration was determined from the previous path data, that is, it matches a configuration attained shortly after the motion was started:

$$\phi = \begin{bmatrix} 1.3328 & -2.0443 & -0.7994 & 1.4801 \\ -1.3123 & 1.029 & -0.7661 \end{bmatrix}^T \text{ [rad].}$$

The results are depicted in Figure 4. It is seen that, indeed, now there is no fast initial motion. But the problem at the end of the motion, due to the vanishing vector \mathbf{c} , remains. This shows that null space minimization yields a poorer performance in terms of spurious arm motion than the SC pseudoinverse technique. For comparison, Figure 5 depicts the SC

pseudoinverse control performance with the new initial configuration. No spurious motion is observed, while the quality of the path remains the same.

Insight about base attitude reaction under SC pseudoinverse control and SC null space minimization control is obtained from the graphs in Figure 6. Figure 6 (a) is for the non-optimal initial configuration, while Figure 6 (b) is for the optimal one. It is apparent that the SC null space minimization technique outperforms the SC pseudoinverse one. But the gain through the former approach seems not to be that big to diminish the significant disadvantage of spurious arm motion due to the vector \mathbf{c} singularity.

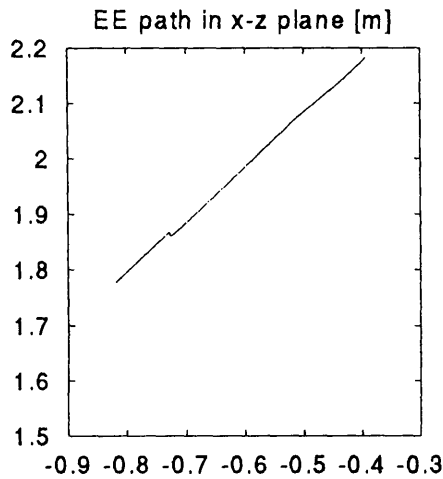
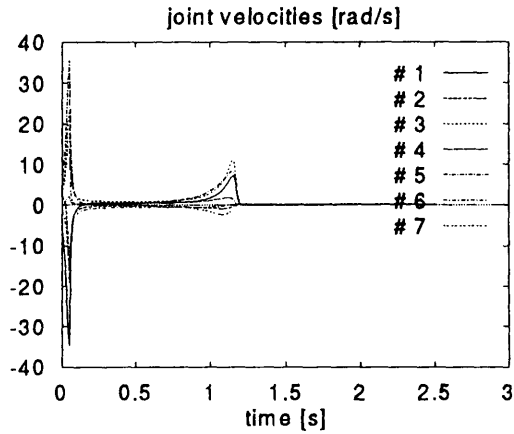


Fig. 3: Motion under SC null space minimum disturbance control with non-optimal initial configuration.

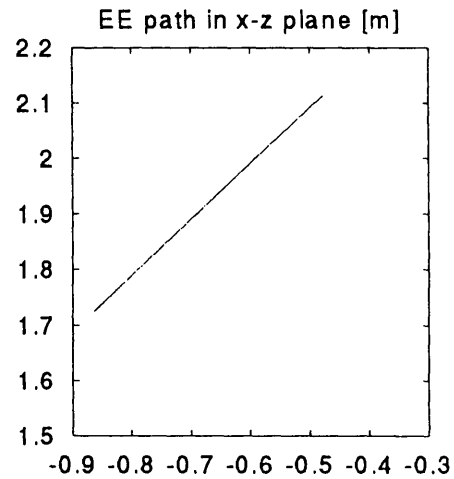
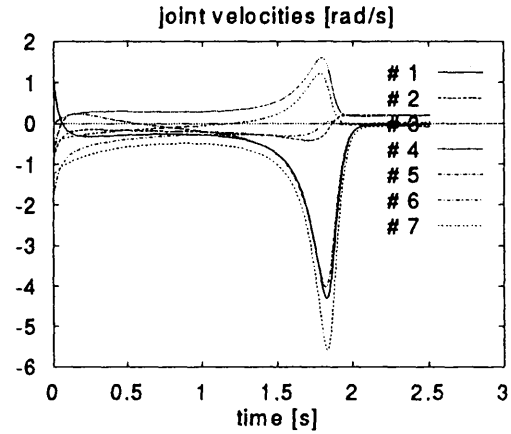


Fig. 4: Motion under SC null space minimum disturbance control with optimal initial configuration.

CONCLUSIONS

We analyzed the performance of a 7 DOF free-flying robot under velocity control. Under conventional pseudoinverse and null space redundancy resolution, the system can be easily destabilized due to the algorithmic singularities. Therefore, we proposed a singularity-consistent solution to the problem. Under this technique no instabilities are observed. Further on, we compared two SC redundancy resolution techniques: one based on the pseudoinverse of the generalized Jacobian, and another one, based on null space minimization of base attitude disturbance. Although the latter method outperforms the pseudoinverse in terms of disturbance minimization, this is done at the expense of spurious arm motions. And the gain from the minimization is not sufficient to diminish the disadvantage. We

conclude that SC pseudoinverse control is a suitable approach to redundancy resolution for a teleoperated arm in space.

APPENDIX

Notations are presented in the form of the Space-Dyn simulation package¹⁵. The location of link centroids of the free-flying robot in [m] are:

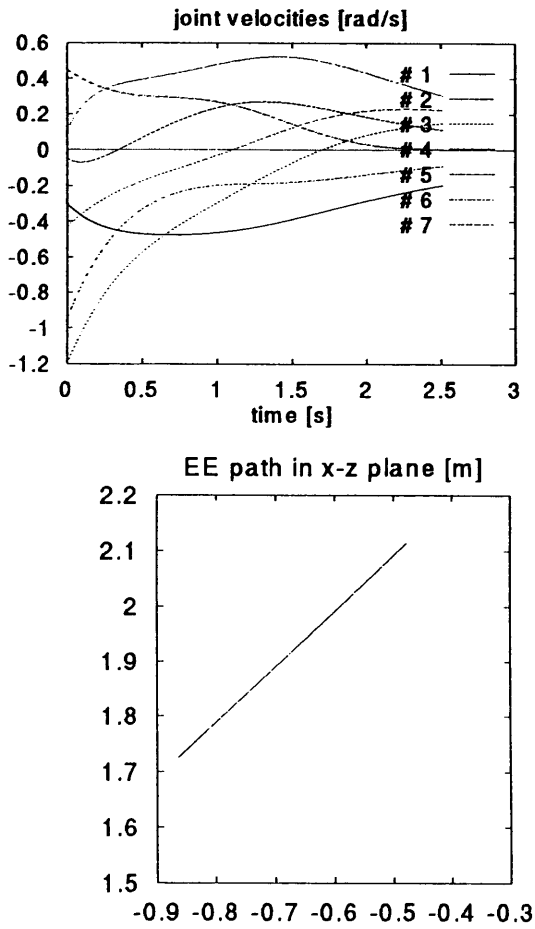


Fig. 5: Motion under SC pseudoinverse control with the optimal initial configuration.

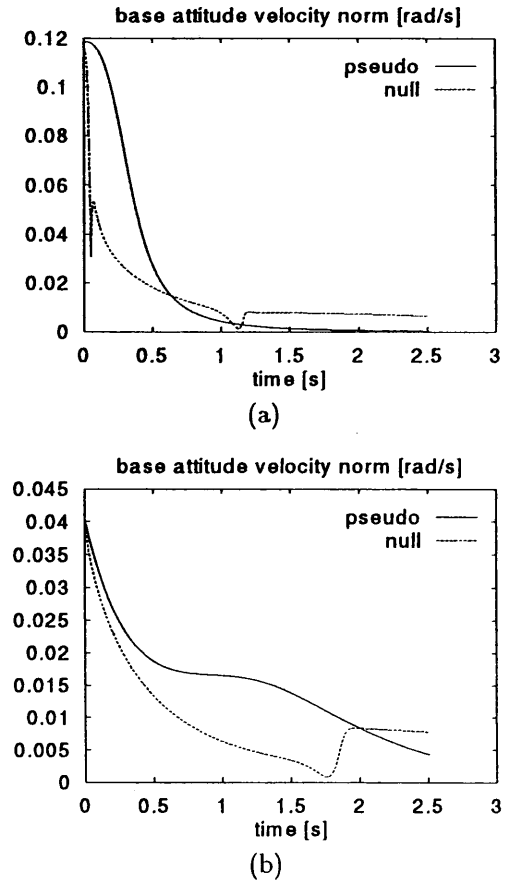


Fig. 6: Base attitude reaction under SC pseudoinverse control and SC null space minimization control: (a) non-optimal initial configuration; (b) optimal initial configuration.

$cc(:,1,1) = [0 \ 0 \ -0.2]'$;
 $cc(:,2,2) = [0 \ 0 \ 0]'$;
 $cc(:,3,3) = [0 \ 0 \ -0.3]'$;
 $cc(:,4,4) = [0 \ 0 \ 0]'$;
 $cc(:,5,5) = [0 \ 0 \ -0.3]'$;
 $cc(:,6,6) = [0 \ 0 \ 0]'$;
 $cc(:,7,7) = [0 \ 0 \ 0.05]'$;
 $cc(:,1,2) = [0.12319 \ 0 \ 0.2]'$;
 $cc(:,2,3) = [-0.10795 \ -0.5461 \ 0]'$;
 $cc(:,3,4) = [-0.07938 \ 0 \ -0.3]'$;
 $cc(:,4,5) = [0.07938 \ 0.5461 \ 0]'$;
 $cc(:,5,6) = [-0.0492 \ 0 \ -0.3]'$;
 $cc(:,6,7) = [0.0492 \ 0 \ 0.05]'$

Base mass is $m_0 = 2469$ [kg]. Base inertia is $I_0 = \text{diag}[7010, 2320, 6200]$ [kgm²]. The mass of each manipulator link is 20 [kg], except the last link, with mass of 37 [kg]. Manipulator link inertia tensors, expressed in [kgm²], are:

$I_1 = \text{diag}[0.2452, 0.2452, 0.1]$
 $I_2 = \text{diag}[0.1, 1.315, 1.315]$
 $I_3 = \text{diag}[0.1, 0.71150, 0.7115]$
 $I_4 = \text{diag}[0.1464, 0.1464, 0.064]$
 $I_5 = \text{diag}[0.1599, 0.1599, 0.064]$
 $I_6 = \text{diag}[0.1599, 0.1599, 0.064]$
 $I_7 = \text{diag}[0.9652, 0.9652, 0.185]$

REFERENCES

- [1] D. L. Akin and R. D. Howard, "The role of free-flight in space telerobotic operations," in Proc. 1993 JSME Int. Conf. on Advanced Mechatronics, Tokyo, Japan, Aug. 1993, pp. 481-486.
- [2] M. Oda, "Coordinated control of spacecraft attitude and its manipulator," in Proc. of the 11th Int. Astrodynamics Symposium, Gifu, Japan, May 19-25, 1996, pp. 265-270.
- [3] D. N. Nenchev, K. Yoshida, and Y. Umetani, "Introduction of redundant arms for manipulation in space," in Proc. 1988 IEEE/RSJ Int. Workshop on Intelligent Robots and Systems (IROS'88), Tokyo, Japan, Oct. 31-Nov. 2, 1988, pp. 679-684.
- [4] D. N. Nenchev, "Redundancy resolution through local optimization: a review," J. Rob. Syst., Vol. 6, No. 6, pp. 769-798, 1989.
- [5] K. Yoshida and D. N. Nenchev, "Space robot impact analysis and satellite-base impulse minimization using reaction null space," in Proc. 1995 IEEE Int. Conf. on Robotics and Automation, Nagoya, Japan, May 21-27, 1995, pp. 1271-1277.
- [6] Y. Tsumaki, D. N. Nenchev, S. Kotera and M. Uchiyama, "Teleoperation based on the adjoint Jacobian approach" IEEE Control Systems Magazine, Vol. 17, No. 1, pp. 53-62, Feb. 1997.
- [7] Y. Nakamura and H. Hanafusa, "Inverse kinematic solutions with singularity robustness for robot manipulator control," ASME J. Dynam. Sys. Measurement and Control, Vol. 108, pp. 163-171, 1986.
- [8] C. W. Wampler II, "Manipulator inverse kinematic solutions based on vector formulations and damped least-squares methods," IEEE Trans. on Systems, Man, and Cyb., Vol. SMC-16, No. 1, pp. 93-101, 1986.
- [9] D. N. Nenchev, Y. Tsumaki and M. Uchiyama, "Real-time motion control in the neighborhood of singularities: a comparative study between the SC and the DLS methods," 1999 IEEE Int. Conf. on Robotics and Automation, Detroit, Michigan, USA May 1999, pp. 506-511.
- [10] K. Kreutz, M. Long and H. Seraji, "Kinematic functions for the 7 DOF Robotics Research arm," NASA Conf. on Space Telerobotics, JPL, Vol. 1, pp. 39-48, 1989.
- [11] K. Yoshida and Y. Umetani, "Resolved motion rate control of space manipulators with generalized Jacobian matrix," IEEE Trans. Rob. Automat., Vol. 5, No. 3, pp. 303-314, 1989.
- [12] H. Seraji and R. Colbaugh, "Improved configuration control for redundant robots," Journal of Robotic Systems, Vol. 7, pp. 897-928, 1990.
- [13] Y. Nakamura, H. Hanafusa, and T. Yoshikawa, "Task-priority based redundancy control of robot manipulators," The Int. Journal of Robotics Research, Vol. 6, No. 2, pp. 3-15, 1987.
- [14] D. N. Nenchev, Y. Tsumaki and M. Uchiyama, "Singularity-consistent behavior of telerobots: theory and experiments," Int. J. of Robotics Research, Vol. 17, No. 2, pp. 138-152, 1998.
- [15] K. Yoshida, <http://www.astro.mech.tohoku.ac.jp/spacedyn/index-e.html>